# Ring-laser gyroscope without the lock-in phenomenon

Satoshi Sunada, Shuichi Tamura, Keizo Inagaki, and Takahisa Harayama
*Department of Nonlinear Science, ATR Wave Engineering Laboratories, 2-2-2 Hikaridai Seika-cho Soraku-gun Kyoto 619-0228, Japan*
(Received 19 August 2008; published 19 November 2008)

We theoretically and numerically study the effect of backscattering on rotating ring lasers by employing the Maxwell-Bloch equations. We show that frequency shifts due to the Sagnac effect incorporating the effect of backscattering can be observed without lock-in phenomenon, if the strength of backscattering originating in the bumps of the refractive index is larger than a certain value. It is also shown that the experimental results corresponding to the theoretical ones can actually be obtained by using a semiconductor fiber-optic ring laser gyroscope.

DOI: 10.1103/PhysRevA.78.053822 PACS number(s): 42.81.Pa, 42.65.Sf, 42.60.Da

## I. INTRODUCTION

Ring laser gyroscopes (RLGs) operate laser action on counterpropagating waves and measure their frequency difference (beat frequency) due to the Sagnac effect [1–3]. The main problems for operation are caused by the effects of backscattering and nonlinearity inherent in a gain medium. For instance, when the rotation rate of the RLG is slow, frequency-locking effect induced by backscattering occurs between the counterpropagating waves and eliminates the beat frequency due to the Sagnac effect (Sagnac beat frequency), which is well known as the lock-in phenomenon [2–7]. In conventional He-Ne RLGs, avoiding the lock-in phenomenon has been one of the important issues in order to measure the beat frequency at slow rotation rates, and many investigations have been intensively done for this purpose.

While conventional RLGs utilize a gaseous medium (He-Ne) as a gain medium, a new type of RLG using solid states and a semiconductor material have recently received research attention [8–18]. As is well known, the nonlinearity inherent in these gain media leads to a spatial hole burning effect and suppresses one of the counterpropagating waves due to gain competition (in an ideal ring laser without backscattering and noise sources), unlike in the case of gaseous medium [4,5]. While several theoretical and experimental works exist for solid-state RLGs, many of the investigations have so far focused on overcoming or controlling such a nonlinearity [10,12–14,16].

In this paper, we theoretically and numerically study the effect of backscattering on solid-state and semiconductor RLGs. In the description, we use the Maxwell-Bloch equations, which consists of the Maxwell equations rewritten in a rotating frame of reference and the Bloch equations that have been used as a simple model of solid-state gain media or as a semiconductor material. We show that the RLGs can have a property that the Sagnac beat frequencies are observed without lock-in phenomenon if the strength of backscattering originating in the bumps of the refractive index is larger than a certain value. In this case, we found that the rotation rate dependence of the beat frequency cannot be described by a conventional theory of the Sagnac effect, which gives a linear relation between the beat frequency and the cavity rotation rate [1,2]. Instead, we demonstrate that it follows a formula of frequency difference including the effect of backscattering, which has been derived in Refs. [6,19]. In addition, we report that such rotation rate dependence can actually be observed without the lock-in phenomenon in a semiconductor fiber-optic ring laser gyroscope (S-FOG) [17,18], which is composed of a semiconductor optical amplifier as a gain medium and optical fibers to form a ring cavity.

This paper is organized as follows: In Sec. II, we start with the Maxwell equations in rotating frames of reference and review the eigenmodes of rotating ring cavities with backscattering to explain the Sagnac effect incorporating the effect of backscattering. Then, the Maxwell equations coupled with the Bloch equations (Maxwell-Bloch equations) are introduced to describe the nonlinear interaction between the light field and a gain medium. We analyze the lock-in phenomenon by expanding the Maxwell-Bloch equations by the eigenmodes of a rotating ring cavity with backscattering and derive the critical backscattering strength, above which the lock-in phenomenon does not occur. In Sec. III, numerical simulations confirm whether the Sagnac beat frequency is observed without lock-in phenomenon. The experimental results of S-FOG are reported in Sec. IV. Finally, the summary of this paper is provided in Sec. V

## II. THEORY

Applying the electromagnetic equation of a naturally covariant form (or the general theory of relativity) to rotating ring cavities yields the Maxwell equations generalized to a noninertial frame of reference in uniform rotation with angular velocity vector [6,20–22]. Assuming that the vector is perpendicular to the plane where there is a ring cavity and that the light propagates one dimensionally along the ring cavity, the following equation can be obtained:

$$\left(\frac{\partial^2}{\partial s^2}-\frac{n^2(s)}{c^2}\frac{\partial^2}{\partial t^2}\right)E(s,t)-2\frac{R\Omega}{c^2}\frac{\partial^2}{\partial s\partial t}E(s,t)$$
$$=2\beta(s)\frac{\partial}{\partial t}E(s,t)+\frac{4\pi n^2}{c^2}\frac{\partial^2}{\partial t^2}P(s,t)+F_1(s,t), \qquad (1)$$

where $s$ is the coordinate along the ring cavity in a rotating frame of reference with angular velocity $\Omega$. $R[=L/(2\pi)]$ denotes the radius of the ring cavity. $P(s,t)$ is the polarization depending on the nonlinear response of a gain medium inside

 

the cavity, whose expression is given in Sec. II B. Noise $F_1$ is phenomenologically introduced in order to represent thermal fluctuation, quantum noise, cavity vibrations and so on; $\langle F_1(s,t)\rangle=0$ and $\langle F_1(s,t)F_1^*(s',t')\rangle=\sigma_1\delta(s-s')\delta(t-t')$, where $\sigma_1$ is the strength of the fluctuation, and $\langle\cdots\rangle$ denotes a spatial average or a time average. $c$ is the velocity of the light, and $n(s)$ and $\beta(s)$, respectively, denote the refractive index and the background absorption. Throughout this paper, it is assumed that the effect of backscattering from one of the rotating waves to the opposite rotating waves can be described by the bumps of the refractive index and absorption.

### A. Eigenmodes of a rotating ring cavities with backscattering

A key to understanding the effects of backscattering and rotation is to analyze the eigenmode structure of the ring cavities [19,23]. We here review eigenmodes and the difference between the eigenfrequencies in a rotating ring cavity with backscattering, which have been derived in Refs. [6,19], since the eigenmode representation is used in Sec. II C to analyze laser operation of the ring cavity.

The eigenmodes can be described by the following wave equation derived from the Maxwell equation (1) omitting absorption $\beta$, polarization term $P$, and noise term $F_1$:

$$\left(\frac{\partial^2}{\partial s^2}+n^2(s)\frac{\omega^2(\Omega)}{c^2}\right)U(s)+2i\frac{R\Omega\omega(\Omega)}{c^2}\frac{\partial}{\partial s}U(s)=0, \quad (2)$$

where $E(s,t)$ oscillates with frequency $\omega(\Omega)$ as $E(s,t)=U(s)e^{-i\omega(\Omega)t}+$c.c. and $U$ is the wave function of the mode obtained under periodic boundary condition $U(s+L)=U(s)$, where $L$ is the cavity length. Below, it is assumed that the wave functions satisfy orthogonal relation $1/(n_0^2L)\oint U_iU_j^*n^2ds=\delta_{ij}$ up to the first order of $R\Omega/c$. In the above, $L$ is the total length of a ring cavity, and $n_0$ is spatial-averaged refractive index $n_0^2=1/L\oint n^2(s)ds$.

In the case of nonrotating ring cavity $\Omega=0$, Eq. (2) can be reduced to a usual wave equation $[\partial^2/\partial s^2+n^2(s)\omega_j(0)^2/c^2]U_j^0(s)=0$, where $\omega_j(0)$ and $U_j^0$, respectively, denote the eigenfrequency and the wave function of a nonrotating cavity. In particular, when the refractive index is uniformly distributed inside cavity $n(s)=n_0$, it is known that the solutions of the wave equation are clockwise (CW-) rotating wave function and counterclockwise (CCW-) rotating wave function with an identical frequency $\omega_0=(ck_0=)2\pi mc/(n_0L)$, where $m$ is an integer $(m=1,2,\ldots)$.

However, such modes with identical frequency cannot generally be described as eigenmodes when the spatial distribution of refractive index $n(s)$ is nonuniform, i.e., there is a bump of the refractive index in the ring cavity: $\Delta n^2(s)(=n^2-n_0^2)\neq 0$. In this case, the bump of the refractive index causes a linear coupling between the CW- and CCW-rotating wave modes due to backscattering and the wave functions of the eigenmodes change into two standing waves [19,23]. Then, the degenerate frequency is split into two frequencies. For instance, when the bumps of refractive index $\Delta n^2\ll 1$ are so small, the frequency splitting $\Delta\omega_0[=\omega_1(0)-\omega_2(0)]$ can be associated with the strength of the backscattering which has a conservative nature, as follows [19,23]:

$$\Delta f_0=\frac{\Delta\omega_0}{2\pi}\approx\frac{c}{n_0\pi L}\sqrt{\gamma}, \quad (3)$$

where $\gamma$ is the intensity-reflection coefficient of the backscatters $(\gamma\ll 1)$. Then the two standing wave modes with the splitting eigenfrequencies are described as follows:

$$U_1^0(s)=\sqrt{2}\cos n_0k_0s, \quad U_2^0(s)=\sqrt{2}\sin n_0k_0s. \quad (4)$$

Moreover, when the cavity is rotated, the rotation affects the standing wave modes of a nonrotating cavity and causes shifts of their eigenfrequencies. The effects can be shown by applying the perturbation theory for nearly degenerate states typically used in quantum mechanics to Eq. (2) [24–26]. Based on the perturbation theory, the eigenmodes in a rotating cavity with backscattering can be represented as the superposition of the nearly degenerate modes as

$$U=c_1U_1^0(s)+c_2U_2^0(s), \quad (5)$$

where the ratio of coefficients $c_1$ and $c_2$ is obtained as

$$c_2/c_1=i\frac{\hat{S}\Omega}{\pm\sqrt{\hat{S}^2\Omega^2+\Delta\omega_0^2}-\Delta\omega_0}. \quad (6)$$

Then frequency $\omega_j(\Omega)$ of eigenmode $j$ $(j=1,2)$ newly produced by cavity rotation up to the first order of $R\Omega/c$ is described as

$$\omega_1(\Omega)=\omega_0+\frac{1}{2}\sqrt{\hat{S}^2\Omega^2+\Delta\omega_0^2}, \quad (7)$$

$$\omega_2(\Omega)=\omega_0-\frac{1}{2}\sqrt{\hat{S}^2\Omega^2+\Delta\omega_0^2}, \quad (8)$$

where $\Delta\omega_0$ is the frequency difference between modes of the nonrotating cavity and $\hat{S}$ is the so-called scale factor, which can be represented as $\hat{S}=\frac{1}{n_0^2c\pi}\left|\oint U_1^0\frac{\partial}{\partial s}U_2^0ds\right|\approx 2\omega_0R/(n_0c)=4\omega_0A/(n_0cL)$, where $A$ is the area bounded by the ring cavity [2]. From Eqs. (7) and (8), frequency difference $\Delta f_\Omega=|\Delta\omega_2(\Omega)-\Delta\omega_1(\Omega)|/(2\pi)$ can finally be obtained as follows [6,19]:

$$\Delta f_\Omega=\frac{\Delta\omega_\Omega}{2\pi}=\sqrt{S^2\Omega^2+\Delta f_0^2}, \quad (9)$$

where $S=\hat{S}/(2\pi)$ and $\Delta f_0=\Delta\omega_0/(2\pi)$.

If there are no backscatters in a ring cavity (i.e., $\Delta f_0=0$), the eigenmodes are described as CW- and CCW-rotating waves, and frequency difference $\Delta f_\Omega$ is proportional to rotation rate $\Omega$ [1,2]. However, in the case of a ring cavity with backscattering, as seen in Eq. (9), the relation between frequency difference $\Delta f_\Omega$ and rotation rate $\Omega$ is not proportional, and it is modified by the effect of backscattering $\gamma$. Then as seen in Eq. (5), the modes are expressed as superposed standing waves with the ratio shown in Eq. (6). This is the Sagnac effect in a ring cavity with backscattering.

### B. Model of a gain medium

Next, we discuss the case of a ring laser taking into account the effect of a gain medium in order to examine how the Sagnac effect is observed in this case.

To describe a gain medium in interaction with the light field, we use the well-known optical Bloch equations, which have been employed as a simple model of solid-state gain medium or as semiconductor gain medium:

$$\frac{\partial}{\partial t}\rho(s,t) = -(\gamma_\perp + i\omega_t)\rho(s,t) - i\kappa W(s,t)E(s,t) + F_2(s,t), \tag{10}$$

$$\frac{\partial}{\partial t}W(s,t) = -\gamma_\parallel(W(s,t) - W_\infty) - 2i\kappa E(s,t)(\rho(s,t) - \rho^*(s,t)) + F_3(s,t), \tag{11}$$

where it is assumed that the medium is not influenced by rotation. In the above, $\rho$ and $W$ denote microscopic polarization and population inversion, respectively. The two relaxation parameters, $\gamma_\perp$ and $\gamma_\perp$, are the transversal relaxation and longitudinal relaxation rates, respectively. $\omega_t$ is the transition frequency between two level medium, and $W_\infty$ is the pumping power. Noises $F_2$ and $F_3$ are introduced phenomenologically in order to represent thermal and pumping fluctuations:

$$\langle F_i(s,t)\rangle = 0,$$

$$\langle F_i(s,t)F_j^*(s',t')\rangle = \sigma_i\delta_{ij}\delta(s-s')\delta(t-t'), \tag{12}$$

where $\sigma_i$ $(i=1,2,3)$ is fluctuation strength. The Bloch equations (10) and (11) are coupled with the Maxwell Eq. (1) through the following relation between microscopic polarization $\rho$ and macroscopic one $P$:

$$P(s,t) = N(s)(\rho(s,t) + \rho^*(s,t))\kappa\hbar, \tag{13}$$

where $\kappa$ is a real number characterizing the electric-dipole coupling, and $N(s)$ is the atomic number density described as $N(s)=N_a\Theta(s)$, where $\Theta(s)$ is a step function that is 1 inside a region of a gain medium and zero outside it.

Equations (1), (10), (11), and (13) are the fundamental ones describing the light field and the gain medium mentioned above.

### C. Two mode operation in rotating ring lasers

In analyzing the dynamics of Eqs. (1), (10), (11), and (13) in ring lasers, we expand these equations by the eigenmode basis of a rotating cavity derived in Sec. II A and derive the amplitude and the phase equations of the modes, although in conventional theoretical approaches, CW- and CCW-rotating wave basis has been frequently used [2–6,11–15]. As demonstrated in Ref. [19,23], using the eigenmode basis makes it possible to simply discuss dynamical behaviors of ring lasers.

To focus on the effect of a gain medium, we here omit noise terms $F_i$ $(i=1,2,3)$ in the Maxwell-Bloch equations (1), (10), (11), and (13), and assume that electric field $E(s,t)$ are described by two eigenmodes $U_j$ $(j=1,2)$ as follows:

$$E(s,t) = \tilde{E}(s,t)e^{-i\omega_0 t} + \text{c.c.} = \sum_{j=1,2} E_j(t)e^{i\phi_j(t)}U_j(s)e^{-i\omega_0 t} + \text{c.c.}, \tag{14}$$

where $E_j$ and $\phi_j \in \mathbb{R}$ denote the amplitude and the phase of the mode $j$ of a rotating ring cavity, respectively. Then we assume that frequency $\omega_0$ is close to the transition frequency $\omega_t$ of the gain medium, $|\omega_0-\omega_t|/\omega_t \ll 1$.

In this case, solving Eqs. (10), (11), and (13) by a perturbational method for small electric field yields $P \approx -i\alpha_0\tilde{E}W\Theta + \text{c.c.}$ and $W=W_\infty(1-\beta_0|\tilde{E}|^2)+O(|\tilde{E}|^4)$, where $\alpha_0=2\pi N_a\kappa^2\hbar\omega_0/\gamma_\perp$ and $\beta_0=4\kappa^2/(\gamma_\perp\gamma_\parallel)$. By substituting them in the Maxwell equation (1) and using the following orthogonal relation $1/(n_0^2L)\oint U_i^*U_jn^2(s)ds=\delta_{ij}+O(|R\Omega/c|^2)$, where $n_0$ is the spatial-averaged refractive index, $n_0^2=1/L\oint n^2ds$, we can obtain the following equations for amplitude $E_j$:

$$\frac{d}{dt}E_j = (g_j - s_jE_j^2 - c_{12}E_{3-j}^2)E_j - M_j^c\cos\Psi - M_j^s\sin\Psi - \bar{M}_j\cos(2\Psi+\theta_\chi), \tag{15}$$

where "net-gain" coefficient $g_j$, self-saturation coefficient $s_j$, and cross-saturation coefficient $c_{12}$ are given in Table I. $\Psi$ is the phase difference, i.e., $\phi_2-\phi_1$. Modulation amplitudes $M_j^c$, $M_j^s$, and $\bar{M}_j$ are described as

$$M_j^c = (|\gamma_{12}|\cos\theta_\gamma + 3|\xi_j|\cos\theta_jE_j^2 + |\xi_{3-j}|\cos\theta_{3-j}E_{3-j}^2)E_{3-j}, \tag{16}$$

TABLE I. Coefficients in Eqs. (15)–(17) and (19).

| Coefficient | Physical content |
|---|---|
| $g_j=\alpha_0 t_jW_\infty-\gamma_{jj}$ | Linear net gain |
| $s_i=\frac{\beta_0W_\infty}{n_0^2L}\oint\Theta\lvert U_i\rvert^4n^2ds$ | Self-saturation |
| $c_{12}=\frac{2\beta_0W_\infty}{n_0^2L}\oint\Theta\lvert U_1\rvert^2\lvert U_2\rvert^2n^2ds$ | Cross-saturation |
| $\xi_j=\frac{\beta_0W_\infty}{n_0^2L}\oint\Theta\lvert U_j\rvert^2U_i^*U_{3-j}^2n^2ds$ | Modulation |
| $\chi=\frac{\beta_0W_\infty}{n_0^2L}\oint\Theta U_1^{*2}U_2^2n^2ds$ | Modulation |
| $\alpha_0=\frac{2\pi N_a\kappa^2\hbar\omega_0}{\gamma_\perp}$ | First-order factor |
| $t_j=\frac{1}{n_0^2L}\oint\Theta\lvert U_i\rvert^2n^2ds$ | Light-medium coupling |
| $\gamma_{ij}=\frac{c^2}{n_0^2L}\oint\beta U_i^*U_jds$ | Dispersive coupling |
| $\beta_0=\frac{4\alpha_0\kappa^2}{\gamma_\perp\gamma_\parallel}$ | Third-order factor |
| $n_0^2=\frac{1}{L}\oint n^2ds$ | Averaged refractive index |

$$M_j^s = (-1)^{3-j}(|\gamma_{12}|\sin\theta_\gamma + 3|\xi_j|\sin\theta_j E_j^2 - |\xi_{3-j}|\sin\theta_{3-j}E_{3-j}^2)E_{3-j}, \tag{17}$$

$$\bar{M}_j = |\chi|E_{3-j}^2 E_j, \tag{18}$$

where $\theta_\gamma$, $\theta_j$, and $\theta_\chi$ are the arguments of $\gamma_{12}$, $\xi_j$, and $\chi$, respectively.

On the other hand, the dynamics of phase difference $\Psi(=\phi_2-\phi_1)$ is described as

$$\frac{d}{dt}\Psi = -\Delta\omega_\Omega + H(\Psi), \tag{19}$$

where $\Delta\omega_\Omega[=\omega_2(\Omega)-\omega_1(\Omega)]$ is the frequency difference between the two modes, as shown in Eq. (9). $H$, which is a periodic function of $\Psi$ (period $2\pi$), can be described as follows:

$$H(\Psi) = |\gamma_{12}|\frac{E_1^2+E_2^2}{E_1E_2}\sin(\Psi+\theta_\gamma) + |\chi|(E_1^2+E_2^2)\sin(2\Psi+\theta_\chi), \tag{20}$$

when amplitudes $E_1$ and $E_2$ are small enough and $\xi_1 \approx \xi_2^* \ll 1$.

The solutions of Eqs. (15) and (19) can be mainly classified into two: One is a stable stationary solution with constant amplitudes and a constant phase difference, and the other is with time-dependent phase difference and amplitude modulating with the phase difference. The distinction can be clearly made by examining Eq. (19), which describes the time evolution of the phase difference.

Note that the form of Eq. (19) resembles with the well-known locking equation [2–6]. This means that the solution of Eq. (19) markedly depends on the relative strengths of $\Delta\omega_\Omega$ and $\max|H(\Psi)|$, where $\max|H(\Psi)|$ denotes the maximal value of $|H(\Psi)|$, which is obtained by solving the stationary equations of $dE_i/dt=0$. For instance, in the case of $\Delta\omega_\Omega < \max|H(\Psi)|$, Eq. (19) has stable fix points given by the solution of $d\Psi/dt=0$. According to definition of $\Psi$, condition $d\Psi/dt=0$ implies that the frequency difference between modes 1 and 2 equals zero, i.e., the lasing frequency of mode 1 becomes identical with that of mode 2, which is the lock-in (frequency locking) phenomenon. On the other hand, when condition $\Delta\omega_\Omega \gg \max|H(\Psi)|$ is satisfied, the lock-in phenomenon does not occur. Thus, phase difference $\Psi$ can be approximately described as $\Psi(t) \approx -\Delta\omega_\Omega t + \Psi_0$, where $\Psi_0$ is an initial phase, while the amplitudes $E_j$ $(j=1,2)$ of the lasing modes oscillate with frequency $\Delta\omega_\Omega$ through the modulation terms of Eq. (15) [18].

Here we emphasize that frequency difference $\Delta\omega_\Omega$ in Eq. (19) not only depends on rotation rate $\Omega$ but also on the strength of conservative backscattering $\gamma$. As shown in Eq. (9), $\Delta\omega_\Omega$ never becomes zero even at rotation rate $\Omega=0$ when there are backscatters inside the ring cavity. This means that the lock-in phenomenon does not occur even at rotation rate $\Omega=0$ if frequency splitting $\Delta\omega_0$ is large enough to satisfy condition:

$$\Delta\omega_0 > \max|H(\Psi)|_{\Omega=0} \equiv \Delta\omega_c. \tag{21}$$

This condition is rewritten using Eq. (3) as follow:

$$\gamma > \gamma_c = \frac{n_0^2L^2}{4c^2}\Delta\omega_c^2. \tag{22}$$

Although criterion $\Delta\omega_c$ is too complicated to be analytically expressed for general cases, it has the simple form for a case where the wave functions of the two modes can be expressed by Eq. (4) because of $\gamma \ll 1$ and where wavelength $2\pi/k_0$ of the light is shorter than the size of the ring cavity $k_0\int\Theta(s)ds \gg 1$. Therefore $g_1 \approx g_2 = g$ and $s_1 \approx s_2 = s$. By solving equation $dE_i/dt=0$ under such conditions, we can derive criterion $\Delta\omega_c$,

$$\Delta\omega_c = 2\max\left|\frac{|\gamma_{12}|(K-1)\sin\Psi + g\sin 2\Psi}{K+\cos 2\Psi}\right|, \tag{23}$$

where $K=s/\chi+2\approx 5$. In the case of (dispersive coupling) $\gamma_{12} \gg g$ (linear net gain), since $H(\Psi)$ has maximal value at $\Psi_m=\pi/2(2m+1)$, where $m$ is an integer, Eq. (23) is reduced to $\Delta\omega_c=2|\gamma_{12}|$, while in the case of $\gamma_{12} \ll g$, it is reduced to $\Delta\omega_c=2g/\sqrt{K^2-1}$ [27], where $H(\Psi)$ takes the maximal value at $\Psi_m=m\pi-1/2\arctan\sqrt{K^2-1}$.

It is known that, in the case of conventional RLGs using a gaseous medium, disappearance of frequency difference is caused by nonlinear phenomena such as lock-in in low rotation rate regime [2,3,6,7]. However, this result means that, if conditions (21) or (22) are satisfied, solid-state RLGs will have a property that the lock-in phenomenon is naturally avoided. It can be concluded that the frequency difference $\Delta\omega_\Omega$ described by Eq. (9) without the lock-in phenomenon can be observed even at arbitrary slow rotation rate.

## III. NUMERICAL SIMULATIONS

In the preceding section, we derived the amplitude and the phase-difference equations under two mode operation by expanding the Maxwell-Bloch equations by the eigenmodes of a rotating ring cavity with backscattering, and discuss the occurrence of lock-in phenomenon. Note that a perturbation theory for $\rho$ and $W$ and several approximations, including $E_i \ll 1$, are employed in the derivation. Additionally, noise terms $F_i$ are omitted. Thus, it is needed to check the validity of the theoretical predictions obtained in the preceding section by the Maxwell-Bloch equations (1) and (10)–(13) including noise terms and full-order nonlinearity of a gain medium. In this section, we restrict ourselves to discuss the lock-in phenomenon by the numerical simulations. Detailed discussions of the effect of noises on lasing dynamics will be reported elsewhere.

Note that it will take a very long time to simulation the Maxwell-Bloch equations because the fast oscillation as well as the slowly varying envelop of the light field are simulated. The fast oscillation part of the light field has the constant frequency, which is very close to the transition frequency $\omega_t$. Thus it is possible to separate the slowly varying part from the fast oscillation part in order to investigate the dynamics of rotating ring lasers.

Let us suppose $\tilde{E}$ and $\tilde{\rho}$ to be the slowly varying envelope of the electric field and the polarization field as $E=\tilde{E}e^{-i\omega_0 t}$ +c.c. and $\rho=-i\tilde{\rho}e^{-i\omega_0 t}$, where the rotation wave approximation (RWA) is taken into consideration for the polarization. Applying the slowly varying approximation for time to Maxwell-Bloch Eqs. (1), (10), (11), and (13) yields the following equations:

$$\frac{\partial}{\partial t}\tilde{E}=\frac{i}{2}\left(\frac{\partial^2}{\partial s^2}+\frac{n^2(s)}{n_0^2}+2i\frac{\Omega_D}{n_0}\frac{\partial}{\partial s}\right)\tilde{E}-\tilde{\beta}\tilde{E}+\eta(s)\tilde{\rho}+\tilde{F}_1(s,t), \tag{24}$$

$$\frac{\partial}{\partial t}\tilde{\rho}=-(\tilde{\gamma}_\perp+i\Delta_0)\tilde{\rho}+\tilde{\kappa}W\tilde{E}+\tilde{F}_2(s,t), \tag{25}$$

$$\frac{\partial}{\partial t}W=-\tilde{\gamma}_\parallel(W-W_\infty)-2\tilde{\kappa}(\tilde{E}\tilde{\rho}^*+\text{c.c.})+\tilde{F}_3(s,t), \tag{26}$$

where space and time are made dimensionless by the scale transformation; $(n_0\omega_0/c)s\to s$ and $\omega_0 t\to t$, respectively, and $\tilde{\beta}\equiv\beta c^2/(n_0^2\omega_0)$, $\Omega_D\equiv R\Omega/c$, $\eta(s)\equiv(2\pi N_a\kappa\hbar/n_0^2)\Theta(s)$, $\tilde{\gamma}_\perp\equiv\gamma_\perp/\omega_0$, $\tilde{\gamma}_\parallel\equiv\gamma_\parallel/\omega_0$, $\tilde{\kappa}\equiv\kappa/\omega_0$, $\Delta_0\equiv(\omega_0-\omega_t)/\omega_0$. $\tilde{F}_i$ is noise with the strength of fluctuation $\tilde{\sigma}_i=c^2/(n_0^2\omega_0^2)\sigma_i$.

In our simulations, we chose a ring cavity with (dimensionless) radius $R=10$ composed of a passive region and an active region where there is a gain medium. Then we suppose $n_1$ and $n_2$ to be the refractive index of the passive and active regions, respectively. Length $l$ of the active region is set as $l=(5\sqrt{2}\times10^{-2})L$, where $L$ is the total cavity length $2\pi R$. Then we set the values of most of the system's parameters as follows: $\tilde{\kappa}=0.5$, $W_\infty=2\times10^{-3}$, $\tilde{\gamma}_\perp=5\times10^{-2}$, $\tilde{\gamma}_\parallel=10^{-3}$, $\tilde{\sigma}_j=10^{-7}(j=1,2,3)$, $\Delta_0=0$, and $\tilde{\beta}(s)=\alpha_L\Theta(s)$, where $\Theta(s)$ is a step function that is 1 inside the active region and zero outside it, and $\alpha_L=10^{-3}$.

Here, note that the conservative backscatters are introduced by the variations of the refractive index in this cavity. Since the strength of backscattering $\gamma$ is related to the variation as $\sqrt{\gamma}\propto(n_2^2/n_1^2-1)$, the resonant frequencies of the eigenmodes of a nonrotating cavity are split into two, following Eq. (3). The solid line in Fig. 1 shows the dependence of (dimensionless) frequency splitting $\Delta\omega_0/\omega_0$ on the ratio of the refractive index $n_2^2/n_1^2$.

For various values of $n_2^2/n_1^2$, we numerically integrate Eqs. (24)–(26) to obtain two mode laser operation in the nonrotating ring laser ($\Omega_D=0$). The detailed method of the numerical simulations is shown in the Appendix.

In Fig. 1, we show the $n_2^2/n_1^2$ dependence of the frequency difference between the two lasing modes by closed circles. As seen in this figure, it turns out that there is a zone corresponding to the absence of the frequency difference for $n_2^2/n_1^2\leqslant1.006$. This is because of frequency locking between two modes. The regime ($n_2^2/n_1^2\leqslant1.006$) corresponds to the case when strength $\gamma$ of conservative backscattering is smaller than critical value $\gamma_c$. On the other hand, the frequency difference can be numerically observed without the frequency locking phenomenon for $n_2^2/n_1^2>1.006$, and its value approaches the solid line obtained from Eq. (3). Below,

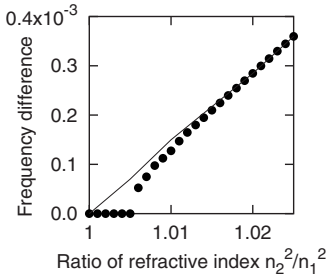


FIG. 1. Frequency difference vs ratio of refractive index $n_2^2/n_1^2$, where $n_1$ and $n_2$ are, respectively, the refractive index of passive and active regions in a nonrotating ring laser ($\Omega=0$). Frequency difference is made dimensionless as $\Delta\omega_0/\omega_0$. Solid line denotes frequency difference between eigenmodes calculated following Eq. (3) in the ring cavity (without a gain medium), while closed circles are results obtained by numerical simulations of Eqs. (24)–(26). Numerical results show that frequency-locking phenomenon occurs and frequency difference becomes zero when $n_2^2/n_1^2$ is less than $\sim1.006$.

we refer to the two regimes, $0<n_2^2/n_1^2\leqslant1.006$ and $n_2^2/n_1^2>1.006$, as locking and unlocking regimes, respectively.

Typical examples of the rotation rate dependence of the frequency difference are shown in Figs. 2(a) and 2(b) for the locking ($n_2^2/n_1^2=1.005$) and unlocking regimes ($n_2^2/n_1^2=1.02$), respectively. The frequency difference calculated by Eq. (9) in each case is represented by the solid line. For the locking regime, when the ring laser is rotated but the rotation rate is small, the frequency-locking phenomenon is still caused and therefore, the frequency difference between the two lasing modes cannot be observed [Fig. 2(a)]. When rotation rate $\Omega_D$ is increased, however, the frequency differ-

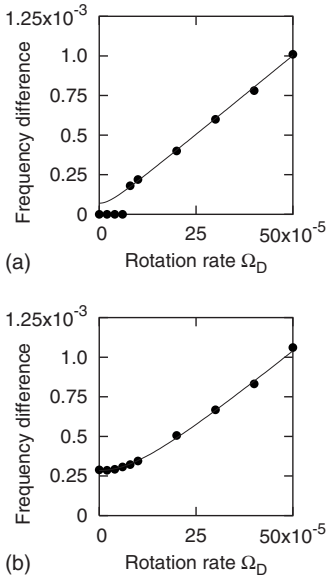


FIG. 2. (Dimensionless) rotation rate $\Omega_D$ vs (dimensionless) frequency difference $\Delta\omega_\Omega/\omega_0$ in rotating ring lasers with locking regime ($n_2^2/n_1^2=1.005$) (a) and unlocking regime ($n_2^2/n_1^2=1.02$) (b). Solid lines denote frequency difference calculated by Eq. (9) in each case, while closed circles denote results obtained from numerical simulations of Eqs. (24)–(26).

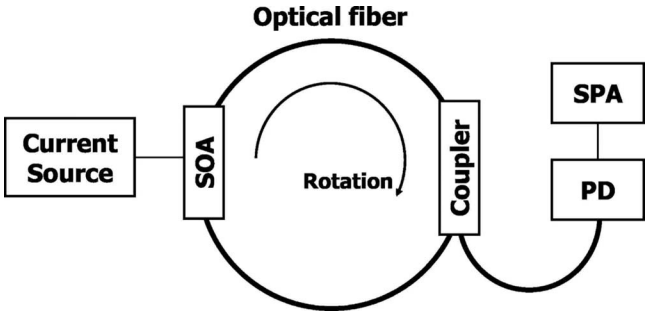


FIG. 3. Experimental setup of semiconductor fiber ring laser gyroscopes (S-FOG): SOA, a semiconductor optical amplifier (its temperature is kept at 25° by a thermocontroller); coupler, 95:5 coupler (5% of energy is extracted only from the CW-output signal inside ring cavity.); PD, photodetector; SPA, rf spectrum analyzer.

ence starts to increase and approaches the values calculated by Eq. (9). The existence of the region corresponding to the absence of the frequency difference might be qualitatively similar with so-called deadband [2]. On the other hand, for the unlocking regime [Fig. 2(b)], as mentioned above, the frequency-locking effect is not caused even at zero rotation rate. As the rotation rate is increased, the frequency difference following Eq. (9) increases without deadband, as shown in Fig. 2(b). These numerical results confirm the theoretical prediction that frequency difference can be observed without the lock-in phenomenon in a ring laser with conservative backscattering.

## IV. EXPERIMENT

Last, let us examine if the theoretical results can actually be obtained in a real experiment. For this purpose, we used a semiconductor fiber optic ring laser gyroscope (S-FOG) [17,18]. The experimental setup is illustrated in Fig. 3. The ring laser part of S-FOG consists of a semiconductor optical amplifier (SOA) as a gain medium and polarization-maintaining fibers to form a ring cavity. Conservative backscattering is mainly caused at the connection point between the SOA and the optical fibers in S-FOG, because there is an air region at the connection point, which leads to substantial changes of the refractive indices at the points [28]. From the return loss measurements, the value of $\gamma$ was approximately estimated as $10^{-5}<\gamma<10^{-4}$. The extraction of the laser output signal from the ring laser part is achieved by a 95:5 coupler, where only 5% energy of the CW-output signal is extracted. It is detected by photodetector PD, as shown in Fig. 3. SPA denotes a rf spectrum analyzer that is used to observe the beat frequency signals of the output signal [29]. The entire system including power supplies and measurement instruments is mounted on a rotation table.

### A. Estimation of $\gamma_c$

To obtain the critical backscattering strength $\gamma_c$ for the S-FOG, it is useful to estimate the parameters (dispersive coupling $\gamma_{12}$ and linear net gain $g$) that determine the $\gamma_c$-value [Eq. (22)].

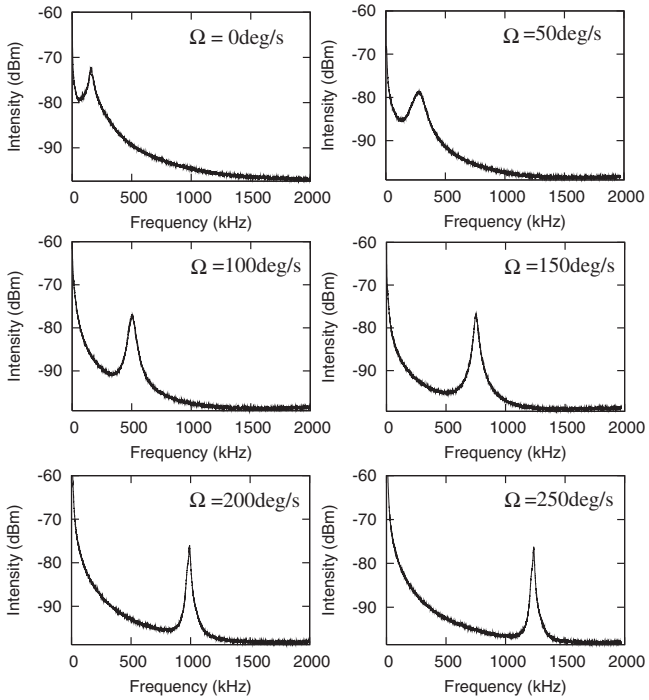


FIG. 4. rf spectrum at each rotation rate Ω (deg/s). Sharp peaks, representing beat frequencies, can be observed in $1/f$-like noise.

Dispersive coupling $\gamma_{12}$ can be calculated on the basis of the definitions shown in Table I as $\gamma_{12} \approx \Gamma/(2n_0kl)|\sin n_0kl \sin\theta| < \Gamma/(2n_0kl)$, where $\Gamma$ is the total loss (typically, $10^5<\Gamma<10^6$ s$^{-1}$) of the ring cavity. $k_0$ and $l$ are, respectively, the wave number of the light and SOA length ($l\approx 1.5$ mm), and $\theta$ is the parameter related to the position of the SOA. For the calculations, we used the wave functions (4) because $\gamma \ll 1$. Using the S-FOG's parameters (lasing wavelength $\lambda \approx 1563.1$ nm, $n_0=1.445$, and $\Gamma \approx 10^6$ s$^{-1}$) with the above equation yields dispersive coupling $\gamma_{12}<10^4$ s$^{-1}$.

Linear net gain $g$ of the SOA can be rewritten as $g=g_0(\alpha-1)$, where $\alpha$ is the normalized pumping power defined by $\alpha=(W_\infty-W_{th})/W_{th}$ ($W_{th}$ is the pumping threshold), and coefficient $g_0$ is estimated as $g_0\approx 1.3\times 10^7$ s$^{-1}$ using the differential gain coefficient of the SOA. When we set normalized pumping strength $\alpha$ as $\alpha=1.06$ in the ring laser of fiber length $L=4.12$ m, linear gain coefficient $g$ is estimated as $g\approx 6.6\times 10^5$ s$^{-1}$. Using this value and values $\gamma_{12}=10^4$ s$^{-1}$, $K=5$ with Eq. (22) yields critical backscattering strength $\gamma_c\approx 7.2\times 10^{-6}$, which is smaller than the measured value of $\gamma(=10^{-5}-10^{-4})$. From these estimations, we expect that the S-FOG satisfies the condition (22) and generates beat frequency signals without the lock-in phenomenon.

### B. Results and discussions

Figure 4 shows the measured rf spectra obtained from the PD output signal at normalized pumping power $\alpha=1.06$, where the spectrum is time averaged to obtain clear beat signals. As predicted by the above estimation, a peak corresponding to the beat frequency can be seen in the rf spectrum even at zero rotation rate ($\Omega=0$ deg/s). Then the peak fre-

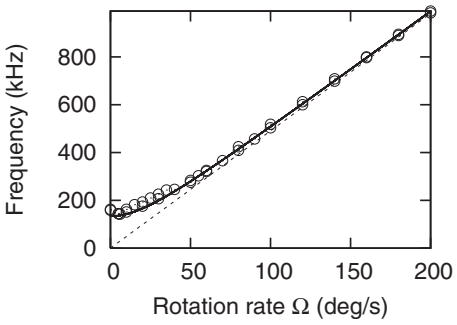


FIG. 5. Beat frequency vs rotation rate. Open circles denote beat frequency obtained from experiments, while dashed line denotes an asymptotic line. Equation (9) is represented by solid line.

quency is changed as the rotation rate is increased. Figure 5 shows the rotation rate dependence of the peak frequencies. The experimental result demonstrates highly linear characteristics only in cases of high rotation rate, while there is substantial deviation from an asymptotic line given by the dashed line for slow rotation rates.

In addition, we confirmed that the similar rotation rate dependence with that shown in Fig. 5 can be observed even when changing the length of an optical fiber of the ring cavity part. According to Eq. (3), the beat frequency observed at zero rotation rate ($\Omega=0$) can be controlled by changing the fiber length. In Fig. 6, we show the dependence of the beat frequency on the fiber length. We find that the dependence can be explained by using Eq. (3) with the assumed backscattering strength $\gamma=7.0\times10^{-5}$, which is given by the solid line in Fig. 6. Assumed $\gamma$ value is consistent with the order of the value $10^{-5}-10^{-4}$ obtained from the return loss measurement. Moreover, to explain the rotation rate dependence of the beat frequency shown in Fig. 5 by using the assumed $\gamma$ value, we superimpose Eq. (9) with $\gamma=7.0\times10^{-5}$ in the solid curve of Fig. 5. It also turns out that the tendency of the experimental results is well reproduced by Eq. (9). Consequently, we conclude that the S-FOGs with $\gamma>\gamma_c$ have a gyro property that the lock-in phenomenon does not occur.

## V. SUMMARY

In summary, we studied the effect of backscattering on rotating ring lasers by using the Maxwell-Bloch equations (1), (10), (11), and (13) and showed that the occurrence of the lock-in phenomenon can be characterized by the strength of the conservative backscattering that originates in the bumps of the refractive index. Particularly, we revealed the existence of critical backscattering strength $\gamma_c$, above which the Sagnac frequency shifts described by Eq. (9) can be observed without the lock-in phenomenon. We also showed that the experimental results corresponding to the theoretical one is actually obtained in a S-FOG. We believe that the property that lock-in phenomenon does not occur is not unique for S-FOGs but universal for RLGs using solid state and semiconductor as gain medium.

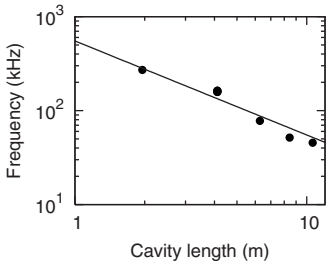


FIG. 6. Beat frequency observed at rotation rate $\Omega=0$ (deg/s) vs cavity length. Closed circles denote beat frequency at zero rotation rate. Equation (3) is represented by a solid line.

## ACKNOWLEDGMENTS

We thank Professor S. Ezekiel, A. Ohno, and Professor K. Hotate for fruitful discussion and valuable comments on S-FOGs. We also thank T. Miyasaka for numerical simulations and S. Shinohara for discussions. This work was supported by the National Institute of Information and Communication Technology of Japan.

## APPENDIX: NUMERICAL SIMULATION METHOD

Let us explain the numerical simulation method of Eqs. (24)–(26). The approximated Maxwell equation (24) has identical form to the Schrödinger equation with absorption $\tilde{\beta}$, polarization $\tilde{\rho}$, and noise $\tilde{F}_1$; it allows us to use the techniques of the symplectic-integrator method [30] to carry out numerical simulations of dynamics.

We divide Eq. (24) into wave propagation, polarization, and noise parts. The time evolution operator of the wave propagation part is given as $U_\tau=e^{-i\hat{H}\tau}$, where $\hat{H}$ consists of the kinetic energy part $\hat{T}=-1/2(\partial^2/\partial s^2+2i\Omega_D/n_0\partial/\partial s)$ and the potential part including linear absorption term $\hat{V}=-n^2/(2n_0^2)-i\tilde{\beta}$ as $\hat{H}=\hat{T}+\hat{V}$. If time $\tau$ is very small, the time-evolution operator can be split based on the symplectic-integrator method as follows:

$$U_\tau = e^{-i\hat{V}\tau/2}e^{-i\hat{T}\tau}e^{-i\hat{V}\tau/2}+O(\tau^3). \tag{A1}$$

The next time-step value of electronic field $\tilde{E}(t+\tau,s)$ is calculated by operating the split $U_\tau$ on the previous time-step value $\tilde{E}(t,s)$ and including the contribution of the polarization term and a noise term up to the first-order correction of $\tau$,

$$\tilde{E}(t+\tau,s)\approx U_\tau\tilde{E}(t,s)+\eta(s)\tilde{\rho}(t,s)\tau+df_1(s,t), \tag{A2}$$

where $df_1=\tilde{F}_1\tau$.

Equation (A2) can be calculated by the following procedures: First, potential part $e^{-i\hat{V}\tau/2}$ is operated on $\tilde{E}(t,s)$ $[\tilde{E}_1(t,s)\equiv e^{-i\hat{V}\tau}\tilde{E}(t,s)]$. Then the Fourier translation of $\tilde{E}_1(t,s)$ is calculated as $\hat{E}_1(t,k)=\oint\tilde{E}_1(t,s)e^{-iks}ds$. Operating $E_1(\hat{t},k)$ to $e^{-i\hat{T}\tau}$ yields the following result:

$$\tilde{E}_2(t,s) = \frac{1}{2\pi}\int e^{-i/2(k^2+2\Omega_D/n_0 k)\tau}\hat{E}_1(t,k)e^{iks}dk. \quad \text{(A3)}$$

Then $e^{-i\hat{V}\tau/2}\tilde{E}_2(t,s)[\equiv\tilde{E}_3(t,s)]$ is obtained. Finally, the next time step $\tilde{E}(t+\tau,s)$ is obtained by adding polarization term $\eta(s)\tilde{\rho}(t,s)\tau$ and noise term $df_1(t,s)$ to $\tilde{E}_3(t,s)$. $df_1$ is generated by converting uniform random numbers generated by the M-sequence technique to normal distribution random numbers by using the Box-Muller formula.

For the Bloch equations, the next time-step value of polarization $\tilde{\rho}(t+\tau,s)$ and population inversion $W(t+\tau,s)$ are calculated by the Euler method,

$$\tilde{\rho}(t+\tau,s) = \tilde{\rho}(t,s) + \frac{d}{dt}\tilde{\rho}(t,s)\tau + df_2(t,s), \quad \text{(A4)}$$

$$W(t+\tau,s) = W(t,s) + \frac{d}{dt}W(t,s)\tau + df_3(t,s), \quad \text{(A5)}$$

where $df_i(t,s)=\tilde{F}_i(t,s)\tau$ $(i=2,3)$ are also generated by the above method.


[1] E. J. Post, Rev. Mod. Phys. **39**, 475 (1967).
[2] W. W. Chow, J. Gea-Banacloche, L. M. Pedrotti, V. E. Sanders, W. Schleich, and M. O. Scully, Rev. Mod. Phys. **57**, 61 (1985).
[3] F. Aronowitz, in *Laser Applications*, edited by M. Ross (Academic, New York, 1971).
[4] M. Sargent III, M. O. Scully, and W. E. Lamb, Jr., *Laser Physics* (Addison-Wesley, Reading, MA, 1974).
[5] M. P. Meystre and M. Sargent III, *Elements of Quantum Optics* (Springer-Verlag, Berlin, 1990).
[6] L. N. Menegozzi and W. E. Lamb, Jr., Phys. Rev. A **8**, 2103 (1973).
[7] C. Etrich, P. Mandel, R. Centeno Neelen, R. J. C. Spreeuw, and J. P. Woerdman, Phys. Rev. A **46**, 525 (1992).
[8] S. K. Kim, H. K. Kim, and B. Y. Kim, Opt. Lett. **19**, 1810 (1994).
[9] S. Huang, K. Toyama, B. Y. Kim, and H. J. Shaw, Opt. Lett. **18**, 555 (1993).
[10] R. Kiyan, S. K. Kim, and B. Y. Kim, IEEE Photonics Technol. Lett. **8**, 1624 (1996).
[11] E. L. Klochan, L. S. Kornienko, N. V. Kravtsov, E. G. Lariontsev, and A. N. Shelaev, Sov. Phys. JETP **38**, 669 (1974).
[12] S. Schwartz, G. Feugnet, P. Bouyer, E. Lariontsev, A. Aspect, and J.-P. Pocholle, Phys. Rev. Lett. **97**, 093902 (2006).
[13] S. Schwartz, G. Feugnet, E. Lariontsev, and J.-P. Pocholle, Phys. Rev. A **76**, 023807 (2007).
[14] S. Schwartz, F. Gutty, G. Feugnet, P. Bouyer, and J.-P. Pocholle, Phys. Rev. Lett. **100**, 183901 (2008).
[15] M. Sorel, P. J. Laybourn, G. Giuliani, and S. Donati, Alta Freq. **10**, 45 (1998).
[16] H. Cao, C. Liu, H. Ling, H. Deng, M. Benavidez, G. M. Peake, G. A. Smolyakov, P. G. Eliseev, and M. Osinski, Appl. Phys. Lett. **86**, 041101 (2005).
[17] K. Inagaki, S. Tamura, H. Noto, and T. Harayama, Proceedings of the 18th International Conference on optical fiber sensors, ME7, 2006.
[18] T. Harayama, S. Sunada, S. Tamura, K. Inagaki, and H. Noto, Proceedings of the 18th International Conference on optical fiber sensors, TuE63 2006.
[19] R. J. C. Spreeuw, R. C. Neelen, N. J. van Druten, E. R. Eliel, and J. P. Woerdman, Phys. Rev. A **42**, 4315 (1990).
[20] J. L. Anderson and J. W. Ryon, Phys. Rev. **181**, 1765 (1969).
[21] E. Landau and E. Lifshits, *The Classical Theory of Fields*, 2nd ed. (Addison-Wesley, Reading, MA, 1962).
[22] C. V. Heer, Phys. Rev. **134**, A799 (1964).
[23] R. Centeno Neelen, R. J. C. Spreeuw, E. R. Eliel, and J. P. Woerdman, J. Opt. Soc. Am. B **9**, 959 (1992).
[24] S. Sunada and T. Harayama, Phys. Rev. A **74**, 021801(R) (2006).
[25] S. Sunada and T. Harayama, Opt. Express **15**, 16245 (2007).
[26] T. Harayama, S. Sunada, and T. Miyasaka, Phys. Rev. E **76**, 016212 (2007).
[27] In the case of $|\gamma_{12}| \gg g$, $\Delta\omega_c$ is similar with a criterion used in Ref. [23], above which an intensity oscillation of CW- and CCW-rotating waves in antiphase occurs due to the two simultaneously oscillating standing-wave modes.
[28] Except for the points, the other connection points in our ring cavity are between optical fibers. However, angled physical contact (APC) connectors are used at the points, and the return loss is less than $10^{-6}$, which can be omitted compared to the return loss at the connection points between SOA and the optical fibers.
[29] This is because beat frequency $\Delta\omega_\Omega$ is transformed to the amplitude oscillation due to the modulation effects of Eq. (15). Thus, an extra directional coupler is not needed to combine the extracted CW- and CCW-output signals in order to produce the beat signals. It has been experimentally confirmed that the amplitude oscillation frequency agrees very well with beat frequency measured by the conventional method with an extra coupler [18].
[30] K. Takahashi and K. S. Ikeda, J. Chem. Phys. **106**, 4463 (1997).